Florida Department of Transportation
Draft Final Report
(For the Period Covering 6/1/2012 – 6/10/2014)

**Impedance-Based Detection of Corrosion in Post-Tensioned Cables:
Phase 2 Extension of Sensor Development**

FDOT Contract No. BDV-31-977-19

FDOT Project Manager: Steven Schein / Ron Simmons

UF Principal Investigator: Mark Orazem, PhD
UF Co-Principal Investigator: David Bloomquist

Graduate Students: Christopher Alexander
                            Yu-Min Chen

Disclaimer

"The opinions, findings, and conclusions expressed in this publication are those of the author(s) and not necessarily those of the Florida Department of Transportation or the U.S. Department of Transportation."

APPROXIMATE CONVERSIONS TO SI UNITS

SYMBOL	WHEN YOU KNOW	MULTIPLY BY	TO FIND	SYMBOL
		LENGTH		
in	inches	25.4	millimeters	mm
ft	feet	0.305	meters	m
yd	yards	0.914	meters	m
mi	miles	1.61	kilometers	km

SYMBOL	WHEN YOU KNOW	MULTIPLY BY	TO FIND	SYMBOL
		AREA		
in²	squareinches	645.2	square millimeters	mm^2
ft²	squarefeet	0.093	square meters	m^2
yd²	square yard	0.836	square meters	m^2
ac	acres	0.405	hectares	ha
mi²	square miles	2.59	square kilometers	km^2

SYMBOL	WHEN YOU KNOW	MULTIPLY BY	TO FIND	SYMBOL
		VOLUME		
fl oz	fluid ounces	29.57	milliliters	mL
gal	gallons	3.785	liters	L
ft³	cubic feet	0.028	cubic meters	m^3
yd³	cubic yards	0.765	cubic meters	m^3
NOTE: volumes greater than 1000 L shall be shown in m^3				

SYMBOL	WHEN YOU KNOW	MULTIPLY BY	TO FIND	SYMBOL
		MASS		
oz	ounces	28.35	grams	g
lb	pounds	0.454	kilograms	kg
T	short tons (2000 lb)	0.907	megagrams (or "metric ton")	Mg (or "t")

SYMBOL	WHEN YOU KNOW	MULTIPLY BY	TO FIND	SYMBOL
		TEMPERATURE (exact degrees)		
ºF	Fahrenheit	5 (F-32)/9 or (F-32)/1.8	Celsius	ºC

SYMBOL	WHEN YOU KNOW	MULTIPLY BY	TO FIND	SYMBOL
		ILLUMINATION		
fc	foot-candles	10.76	lux	lx
fl	foot-Lamberts	3.426	candela/m^2	cd/m^2

SYMBOL	WHEN YOU KNOW	MULTIPLY BY	TO FIND	SYMBOL
		FORCE and PRESSURE or STRESS		
lbf	poundforce	4.45	newtons	N
lbf/in²	poundforce per square inch	6.89	kilopascals	kPa

APPROXIMATE CONVERSIONS TO SI UNITS

SYMBOL	WHEN YOU KNOW	MULTIPLY BY	TO FIND	SYMBOL
LENGTH				
mm	millimeters	0.039	inches	in
m	meters	3.28	feet	ft
m	meters	1.09	yards	yd
km	kilometers	0.621	miles	mi

SYMBOL	WHEN YOU KNOW	MULTIPLY BY	TO FIND	SYMBOL
AREA				
mm²	square millimeters	0.0016	square inches	in²
m²	square meters	10.764	square feet	ft²
m²	square meters	1.195	square yards	yd²
ha	hectares	2.47	acres	ac
km²	square kilometers	0.386	square miles	mi²

SYMBOL	WHEN YOU KNOW	MULTIPLY BY	TO FIND	SYMBOL
VOLUME				
mL	milliliters	0.034	fluid ounces	fl oz
L	liters	0.264	gallons	gal
m³	cubic meters	35.314	cubic feet	ft³
m³	cubic meters	1.307	cubic yards	yd³

SYMBOL	WHEN YOU KNOW	MULTIPLY BY	TO FIND	SYMBOL
MASS				
g	grams	0.035	ounces	oz
kg	kilograms	2.202	pounds	lb
Mg (or "t")	megagrams (or "metric ton")	1.103	short tons (2000 lb)	T

SYMBOL	WHEN YOU KNOW	MULTIPLY BY	TO FIND	SYMBOL
TEMPERATURE (exact degrees)				
ºC	Celsius	1.8C+32	Fahrenheit	ºF

SYMBOL	WHEN YOU KNOW	MULTIPLY BY	TO FIND	SYMBOL
ILLUMINATION				
lx	lux	0.0929	foot-candles	fc
cd/m²	candela/m²	0.2919	foot-Lamberts	fl

SYMBOL	WHEN YOU KNOW	MULTIPLY BY	TO FIND	SYMBOL
FORCE and PRESSURE or STRESS				
N	newtons	0.225	poundforce	lbf
kPa	kilopascals	0.145	poundforce per square inch	lbf/in²

*SI is the symbol for the International System of Units. Appropriate rounding should be made to comply with Section 4 of ASTM E380.
(Revised March 2003)

Technical Report Documentation Page

1. Report No.	2. Government Accession No.	3. Recipient's Catalog No.

4. Title and Subtitle	5. Report Date
Impedance-Based Detection of Corrosion in Post-Tensioned Cables: Phase 2 Extension of Sensor Development	8/2014
	6. Performing Organization Code

7. Author(s)	8. Performing Organization Report No.
Mark Orazem, David Bloomquist, Christopher Alexander, Yu-Min Chen	

9. Performing Organization Name and Address	10. Work Unit No. (TRAIS)
University of Florida Department of Chemical Engineering	
	11. Contract or Grant No.
	BDV-31-977-19

12. Sponsoring Agency Name and Address	13. Type of Report and Period Covered
Florida Department of Transportation 605 Suwannee Street, MS 30 Tallahassee, FL 32399	Draft Final Report – 6/1/2012 – 6/10/2014
	14. Sponsoring Agency Code

15. Supplementary Notes
This final report addresses the contract requirements of both BDK75-977-64 and BDV31-977-19.

16. Abstract
A proof of concept was established for a sensor capable of using indirect impedance spectroscopy to detect the existence of corrosion in post-tensioned tendons. This development was supported by a combination of bench-top experiments performed on synthetic tendons, bench-top experiments performed in synthetic grout pore solutions for the same steel used in tendons, and modeling used to interpret impedance measurements and to simulate the signals obtained by the sensor.

This work showed that indirect impedance can be used to observe differences in the impedance and differentiate between active and passive steel. Sensitivity to localized corrosion was found to be greatest when a current injection electrode is positioned directly above the corroding metal. Since the polarized area of steel was found to be a function of both frequency and the condition of the steel, it will be difficult to extract detailed reaction kinetics from the indirect impedance measurement, but the measurement will identify the presence of active corrosion.

Bench-top measurements performed for ASTM A416 steel in aerated simulated pore electrolytes at pH of 13.6 showed a porous electrode behavior with a low rate of corrosion. In the absence of oxygen, the porous electrode behavior was also observed, but the corrosion rate increased. Experiments performed at elevated temperature showed an increase in the corrosion rate. This work provides guidance for the development of future models for interpretation of indirect impedance measurements.

17. Key Word	18. Distribution Statement
Indirect impedance, Post-tensioned tendons, Corrosion	No Restrictions

19. Security Classif. (of this report)	20. Security Classif. (of this page)	21. No. of Pages	22. Price
Unclassified	Unclassified	37	

Form DOT F 1700.7 (8-72)   Reproduction of completed page authorized

Executive Summary

This final report addresses the contract requirements of both BDK75-977-64 and BDV31-977-19.

The object of this work was to develop a sensor concept that would be suitable for detection of active corrosion in post-tensioned tendons used in segmentally constructed bridges. This work was motivated by observation of tendon failures in some of the 76 major post-tensioned bridges in the state of Florida. A proof of concept was established for a sensor capable of using indirect impedance spectroscopy to detect the existence of corrosion in post-tensioned tendons. This development was supported by a combination of bench-top experiments performed on synthetic tendons, bench-top experiments performed in synthetic grout pore solutions for the same steel used in tendons, and modeling used to interpret impedance measurements and to simulate the signals obtained by the sensor.

This work showed that indirect impedance can be used to observe differences in the impedance and differentiate between active and passive steel. Sensitivity to localized corrosion was found to be greatest when a current injection electrode is positioned directly above the corroding metal. Since the polarized area of steel was found to be a function of both frequency and the condition of the steel, it will be difficult to extract detailed reaction kinetics from the indirect impedance measurement, but the measurement will identify the presence of active corrosion.

Bench-top measurements performed for ASTM A416 steel in aerated simulated pore electrolytes at pH of 13.6 showed a porous electrode behavior with a low rate of corrosion. In the absence of oxygen, the porous electrode behavior was also observed, but the corrosion rate increased. Experiments performed at elevated temperature showed an increase in the corrosion rate. This work provides guidance for the development of future models for interpretation of indirect impedance measurements.

Table of Contents

List of Figures

List of Figures

List of Tables

1. Introduction

External post-tensioned tendons are incorporated in segmental bridge construction to force bridge segments into compression. This allows longer spans between piers and provides increased concrete durability. In this type of bridge construction, precast concrete box-girders are linked outward from bulkheads to form a bridge span between piers. The tendons are located within the inner opening of the box-girders and are run continuously through deviator blocks which help form the profile of the tendon. They consist of multiple 7-wire pre-stressing strands contained within a High-Density Polyethylene (HDPE) duct. The ends of the tendons are anchored and stressed, after which, the duct is filled with cementitious grout.[1] The alkaline grout is designed to provide protection against corrosion, but due to possible voids in the grout and areas of improper mixing, incidents of severe corrosion have occurred. In Florida, the first reported post-tensioned corrosion issue was at the 18-year-old Niles Channel Bridge.[2,3] Similar issues were reported at the 7-year-old Mid Bay Bridge in the Western Panhandle[1,4] and the 15-year-old Sunshine Skyway Bridge in Tampa.[5] A number of studies were commissioned by the Florida Department of Transportation (FDOT) to address these issues. An important conclusion from the study related to the Mid Bay Bridge was that a non-destructive technique for testing corrosion and corrosion risk in these post-tensioned members was needed.

The Federal Highway Administration identified main magnetic flux as a possible nondestructive method for external tendons, but this approach is still in need of development.[6] High-powered magnets are used to induce a static magnetic field in the tendon, and the magnetic flux, which is a function of steel cross-sectional area, is monitored to detect fractures.[7] This method can be used to estimate the cross-sectional area loss of the steel, but it is incapable of determining a corrosion rate. In application to reinforced concrete, many methods have been developed to determine corrosion rate. The most notable of these techniques is the Linear Polarization Resistance method. A small over-potential is applied to the reinforcing steel and the current response is monitored. The polarization resistance of the steel is estimated by dividing the potential by the current response. With the Stern and Geary relationship,[8]

$$i_{\text{corr}} = B / A R_{\text{p}}$$

(1)

the steel polarization resistance R_{p} is used to estimate the corrosion rate based on the Tafel slope B. The Linear Polarization Resistance method requires electrical connection to the steel, but, in reinforced concrete structures, access to the steel can be provided only by cutting through the concrete. To avoid this, research has been done to develop a way to indirectly polarize the steel without an electrical connection. An indirect method has been explored in which an electric field is applied to the surface of the concrete and the induced current indirectly polarizes the steel. An early test of this technique aimed to determine the feasibility of estimating the corrosion rate of steel submerged in distilled water through the application of a current pulse to the electrolyte.[9] An equation to estimate the polarization resistance of the steel from the resistance of the electrolyte and the resistance of the cell measured with the steel present was proposed. The equation was derived based on the assumption that the current ran parallel to the steel. Andrade et al.[10,11] used results of finite element models to propose an analogue circuit that accounts for the polarization behavior of the steel and the properties of the mortar in which the steel is embedded. They showed
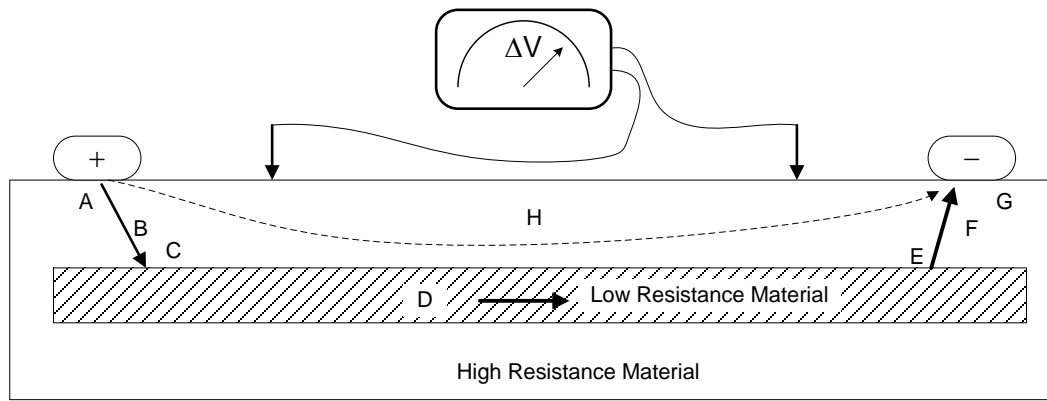
Figure 1. Schematic representation showing the current paths for a highly conductive strand embedded in a more resistive material: (A) interfacial impedance at the positive electrode; (B) ohmic resistance and dielectric response of the resistive material between the positive electrode and the strand; (C) interfacial impedance at the surface of the strand; (D) ohmic resistance of the strand; (E) interfacial impedance at the surface of the strand; (F) ohmic resistance and dielectric response of the resistive material between the negative electrode and the strand; and (G) interfacial impedance at the negative electrode. The letter H signifies the ohmic resistance or dielectric response of the resistive material between the positive and negative electrodes.

that the steel can be indirectly polarized using surface electrodes if the mortar resistivity is sufficiently large.

An alternative to the pulse method is electrochemical impedance spectroscopy, which uses a sinusoidal current or potential perturbation applied to the concrete surface at a range of frequencies to indirectly polarize the steel.[12,13] Monteiro et al. reported using indirect impedance spectroscopy to determine the location and the condition of steel rebar within concrete slabs. They were able to determine qualitatively that the measured surface impedance was a function of the corrosion state of the steel as well as the resistance of the concrete.[12] Keddam et al.[13] showed that at low frequencies (i.e., the d.c. limit) the current flows parallel to the steel; whereas, at high frequencies, the current enters the steel perpendicularly. They found that the zero-frequency limit of the impedance scaled by the resistivity of the grout is a function of the polarization resistance, similarly scaled by the resistivity of the grout. This relationship is independent of the grout resistivity for a defined geometry and electrode configuration. In their application, Keddam et al. were able to neglect the impedance at the working electrode and concrete interface due to the use of wetted sponges applied to the surface of the sample.

The objective of our research is to design a sensor which uses an indirect impedance technique to monitor the integrity of the steel and the grout within a post-tensioned tendon. A schematic representation is provided in Figure 1. The electrical impedance measured between the positive and negative contacts will be influenced by the interfacial impedance at the positive electrode (A); the ohmic resistance or dielectric response of the resistive material between the positive electrode and the strand (B); the interfacial impedance at the surface of the strand (C and E); the ohmic resistance of the strand (D); the ohmic resistance and dielectric response of the resistive material between the negative electrode and the strand (F); and the interfacial impedance at the negative electrode (G). Some current will also flow through the resistive material without passing through the strand. This current will be influenced by the ohmic resistance or dielectric response of the resistive material between the positive and negative electrodes (H). Use of a four-electrode

2

configuration for potential measurement (indicated in Figure 1 by arrows connected to a voltmeter) will eliminate the influence of the interfacial impedances at the positive and negative electrodes. The four-point probe configuration causes the impedance response to reflect the condition of the grout and the strand without the confounding influence of the current injection points.

For the sensor design we will need to determine the appropriate electrode configurations and spacing per tendon geometry, the appropriate electrode materials and contact schemes to the grout, and the appropriate frequency range and perturbation mode to use. The other major objective is to develop a means of interpreting the sensor measurement and determine from that measurement if the steel is corroding. This report will explain the use of simulations to determine which part of the steel is being sensed with a given electrode configuration. This will be done by showing the sensitivity to a locally corroding section by moving the electrodes along the tendon. The significance of this information is that the active steel area sensed will be important in developing a correlation between the indirect impedance measurement and the steel impedance. Through the use of conventional bench-top impedance measurements on ASTM A416M steel in simulated grout pore solutions, the behavior of the steel strands will be determined under different environmental conditions.

2. Research Tasks and Results

A research program was devised to develop a system that assesses the integrity of post-tensioned tendons using indirect impedance spectroscopy. Experiments were performed on synthetic tendons to determine the feasibility of this technique. Finite-element models were used to simulate the indirect impedance, which was compared to the experimental measurements to provide a means of interpreting the results. Conventional impedance experiments were conducted in simulated pore solutions with a disk electrode to determine the impedance behavior of the steel within the environment of the grout. The impedance was analyzed with mathematical models which include physical parameters to describe the behavior of the steel. The information obtained from the regression of the impedance with the mathematical model provided insight into how environmental factors affect the properties of the steel.

The list of tasks is presented below with a summary explanation of accomplishments:
1. *Literature Review.* We learned that the major difficulty in the interpretation of the indirect impedance is determining the area of steel sensed. We learned that distortion in the indirect impedance can occur when the current-injecting electrodes are spaced at a distance much larger than the depth to the steel. We learned the appropriate recipe for simulating the grout pore solution.
2. *Travel to bridge.* On April 26, 2013 we visited the Ringling Causeway Bridge and the Sunshine Skyway Bridge. We learned that post-tensioned tendons were added to the Ringling Bridge after observation of shear cracks in the concrete girders. We noticed tendons that had bulges in them due to failed strands. We took note of the placement of the tendons and identified potential problems to address in the sensor design.
3. *Perform conventional bench-top impedance measurements on simulated and real strands.* Conventional impedance experiments were conducted with an ASTM A416M steel electrode, the same steel used in post-tensioned tendons, in simulated pore solutions. Experiments were conducted in aerated and de-aerated solutions that contained chlorides

as an aggressive medium. It was determined that chlorides do not cause corrosion. However, corrosion rates did increase at elevated temperature.

4. *Perform contact-less bench-top impedance measurements on simulated and real strands.* Impedance experiments were performed on fabricated tendons containing either a proprietary grout or hydrated Portland cement paste as the filler with one steel strand. We were able to determine the appropriate perturbation mode and frequency range to use in our experiments. We determined a reasonable electrode configuration to use and which part of the steel we were sensing as a function of frequency.

5. *Develop mathematical models for interpretation of conventional three-electrode impedance measurements.* A mathematical model was developed to fit the impedance of the steel and simulated pore solution interface which incorporates a porous film model and accounts for the anodic and cathodic impedances.

6. *Develop mathematical models for interpretation of contactless-impedance measurements.* Through the use of finite element simulations it was determined that the polarized area of steel changes with frequency and that the sensing location is directly beneath the working and counter electrodes. A preliminary interpretation technique in which an electrical circuit is used to model the indirect impedance has been tested for the passive case.

7. *Design sensor.* Preliminary guidelines for sensor design were developed. The sensor was found to be sensitive to the condition of the steel under the current-injecting electrodes. A six-inch spacing between current-injection electrodes worked well for a three-inch diameter tendon with a single steel strand. The spacing between current-injection electrodes could be smaller for tendons encasing multiple strands. While initial electrodes were Ag/AgCl, the current design uses iridium-oxide coated titanium.

8. *Prepare final report.*

2.1. Indirect Bench-top Experiments

The indirect impedance technique aims to sense the properties of a conducting element contained within a resistive medium, without an electrical connection to the element. Four electrodes (working, reference 1, reference 2, counter) are placed in an array on the surface of the resistive medium and a perturbation is applied between the working and counter electrodes while the potential response is measured between the reference electrodes. The current takes the path of least resistance through the medium, and is likely to flow through the conducting element, assuming the distance between the electrodes is sufficient.

Experimental tendons were made to resemble a 2-ft. section of a 3-inch diameter tendon to be used to test the indirect impedance method. For the initial ease of interpretation, tendon sections were made with only one steel strand located at the axis of the cylindrical duct. Both a proprietary Sika 300PT cable grout as well as hydrated ordinary Portland cement were used as the filler. In the initial set of tendons, 1-inch holes were cut out of the duct for electrode placement. This allowed some of the pore solution to evaporate, which created resistivity distributions at the electrode locations and made it more difficult to obtain reproducible impedance measurements. Improvements were made to this original design by drilling tapped 1-cm holes into the duct such that the electrodes could be screwed into place, thereby preventing the grout from drying out at these points. Dimensionally stable 0.5-cm diameter titanium rods coated in iridium oxide were used as the electrodes. A conductive solid gel adhesive was used to make a secure electrical connection between the electrode and the grout. The dimensionally stable electrodes were used to measure the indirect impedance as well as to force corrosion. Impedance measurements can be taken by either modulating potential, referred to as potentiostatic modulation, or current, referred to as galvanostatic modulation. Galvanostatic modulation was found to be more reproducible and

less noisy than potentiostatic modulation measurements. Depending on the age of the specimen and the resistivity of the filler material, the appropriate perturbation amplitude is about 10 µA or 10 mV. All measurements were taken at frequencies ranging from 10 mHz - 100 kHz.

2.1.1. Passive Condition

The passive steel condition was established experimentally by properly mixing the grout and allowing it to cure in a dry environment, ensuring that there was no moisture within the duct. Seven electrodes were placed on the surface of the grout, spaced at 3 inches apart from one another. The indirect impedance results are shown in Figure 2 for three different electrode configurations. The numbers in the legend associated with each series correspond to the four electrode locations (working, reference 1, reference 2, and counter). Two time constants are present in our system, one which occurs at a relatively high frequency (10,000 Hz or higher) and is attributed to the working electrode and grout interface, and one at a much lower frequency (1 Hz or less) attributed to the grout and steel interface. In series 1357 the low frequency time constant goes into the negative real impedance quadrant. This distortion is due to the potential distribution through the grout created by the large distance between the electrodes in comparison to the depth to the steel. While the electrodes should be spaced out far enough so that the current is able to reach the steel, these results show that they should not be spaced at distances too much more than the depth to the steel.

Only a portion of the low-frequency time constant is visible within the tested frequency range. Since the interest lies in determining the state of the steel, it would be advantageous to go to the lowest frequency that the instrument allows. Doing so, however, requires much more time and is subject to larger stochastic errors. All of the experiments were performed down to 10 mHz, which takes about 15-20 minutes. Running the experiment down to 1 mHz takes a couple of hours, and, even at this frequency, the full impedance spectrum is not visible. Nevertheless, valuable information can be gleaned from the higher frequency portion of the steel impedance. Results from finite-element simulations showed that the highest frequency portion of the low-frequency arc can provide capacitive properties of the steel which can be used to determine the thickness of the passive film.
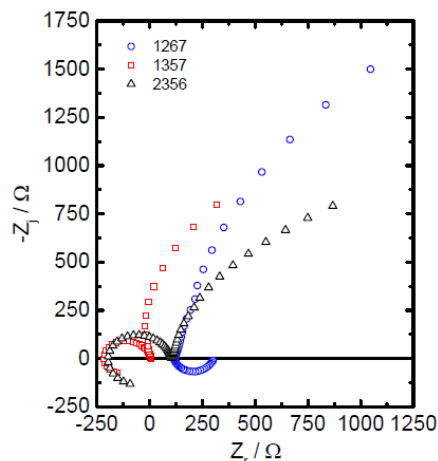

Figure 2. Experimental impedance of cylindrical grout specimen containing one steel strand for three different electrode configurations. The number in the legend corresponds to the electrode contact points along the surface.

2.1.2. Accelerated Corrosion Condition

An accelerated corrosion experiment was performed to determine the difference in the impedance between passive and active steel. A constant 10-V potential was applied to the steel with a counter-electrode serving as a cathode at the center of the 2-ft. fabricated tendon such that the center portion of the steel strand would serve as an anode and, hence, corrode. Due to the large grout resistance, the resulting current was only 40 μA. The potential was applied for 7 days, after which three and four-point impedance measurements were taken along the tendon to determine if a difference could be noticed. The three-point impedance results are presented in Figure 3 in Nyquist format where the counter electrode was moved along the tendon. The series label in the legend corresponds to the distance the counter electrode is placed, either right or left from the corroding location. In all measurements the reference electrode was placed 3 inches from the counter electrode and the steel acted as the working electrode. Seven electrode locations with a 3-inch separation are numbered 1-7. The corrosion site was at electrode location 4. The measurement taken at the corroding site, labeled as 0 in, has the smallest impedance. This result is seen more clearly in Figure 4, where the imaginary impedance is given as a function of frequency.
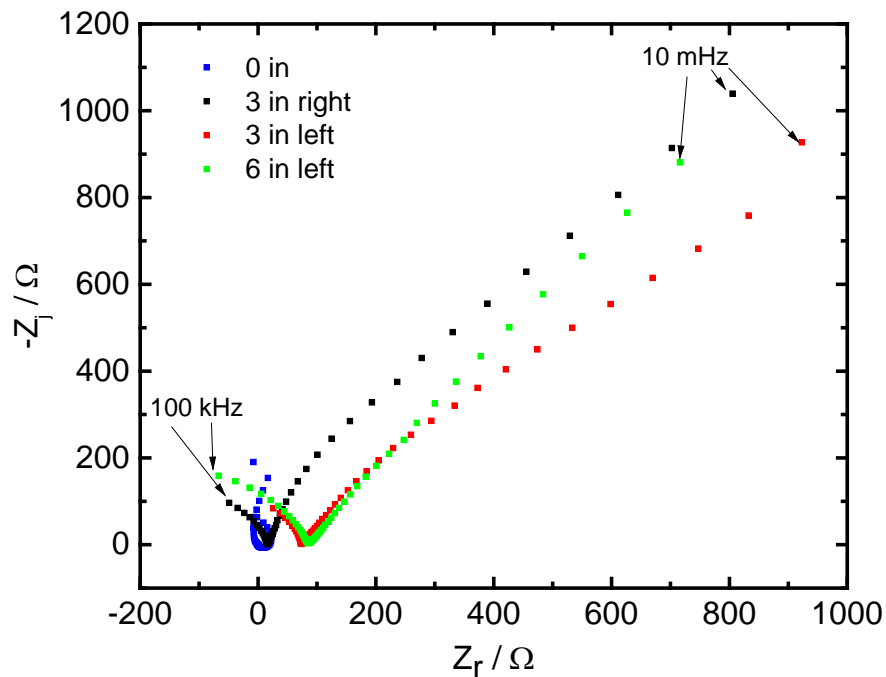
Figure 3. Three-point experimental impedance where the steel is the working electrode and the reference and counter electrodes are placed along the surface of the grout.
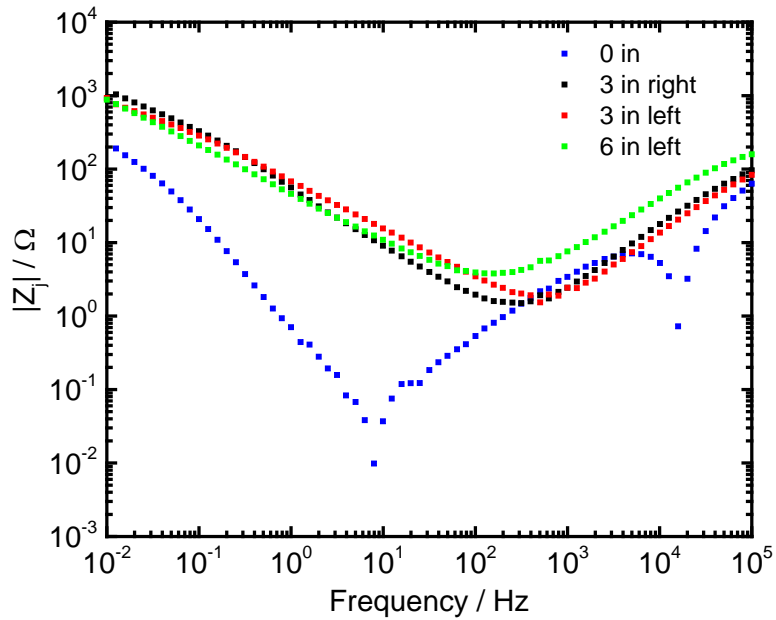
Figure 4. Three-point experimental imaginary impedance as a function of frequency where the steel is the working electrode and the reference and counter electrodes are placed along the surface of the grout.

The indirect impedance measurement was taken along the tendon with equal electrode spacing. The results are presented in Figures 5 and 6. When either the working or counter electrode was at location 4 (1234 or 4567), the impedance was smaller than for the other locations, indicating a possible site of corrosion activity.
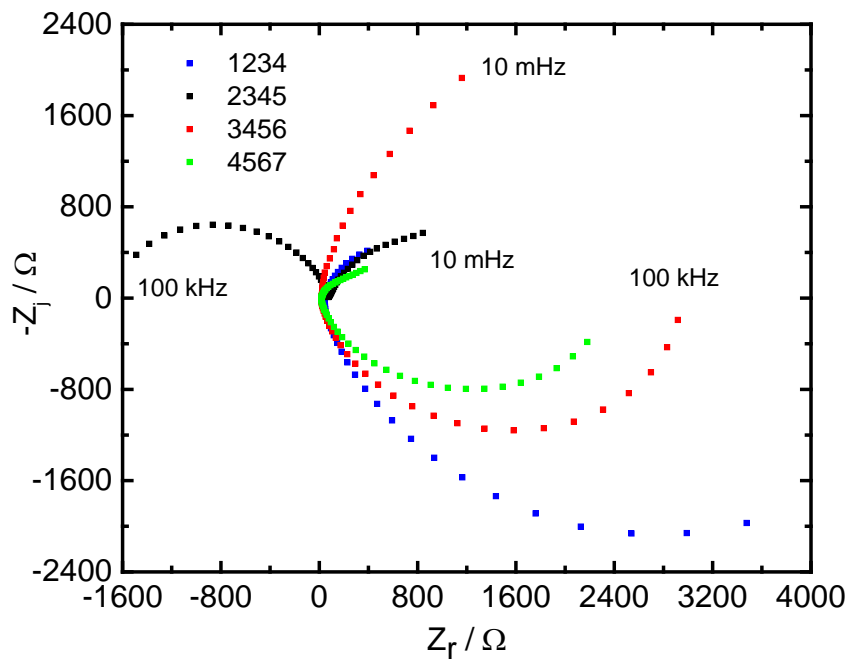
Figure 5. Four-point experimental impedance where the outer two numbers in the legend indicate the positions of the current injection electrodes and the inner two numbers provide the positions of the potential-sense electrodes.
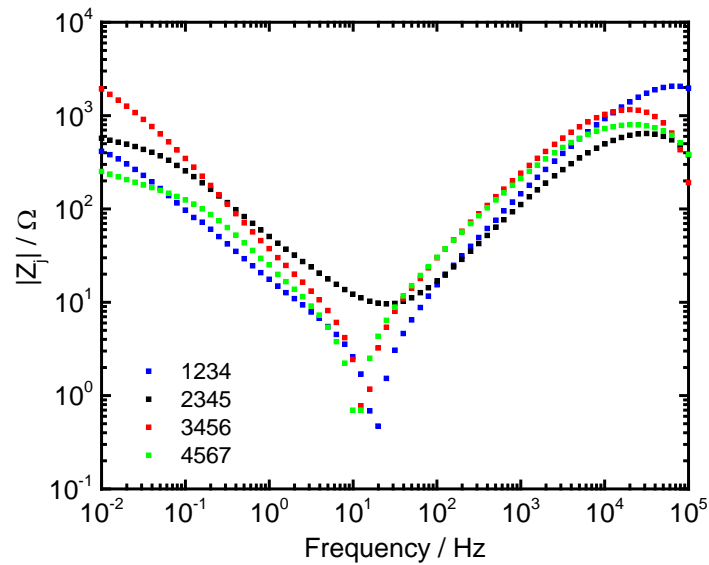
Figure 6. Four-point experimental imaginary impedance as a function of frequency where the outer two numbers in the legend indicate the positions of the current injection electrodes and the inner two numbers provide the positions of the potential-sense electrodes.

The results presented here show that there is a difference in the impedance in locations of corrosion, but this difference is much more prominent in the three-electrode impedance in which there is a direct connection to the steel. As the corrosion gets worse the difference should be more visible. The reduced distance between the casing and the steel and the smaller volume of grout in the field is expected to enhance sensitivity to corrosion.

A second accelerated corrosion experiment was performed on fabricated tendons with freshly cured grout. In this trial the potential was held fixed at 20-V for 1 week. However, it was realized that after the potential difference was removed, the open-circuit potential slowly increased until it reached its initial value indicating that the steel re-passivated. Impedance measurements were then taken during the application of potentials ranging from 0 – 20 V to observe the impedance during the corroding process. The indirect impedance is presented in Nyquist form in Figure 7. At 0 and 1-V the impedance shows a depressed semicircle, but, at higher potentials, the impedance is much smaller and shows little curvature. This difference can also be seen in the imaginary impedance as a function of frequency in Figure 8. The slopes of the 0-V and 1-V measurements are greater than that of the impedance measurements at higher potentials, indicating a higher distribution of time constants which may indicate corrosion, or at least, an area that is less protected than the rest of the steel.
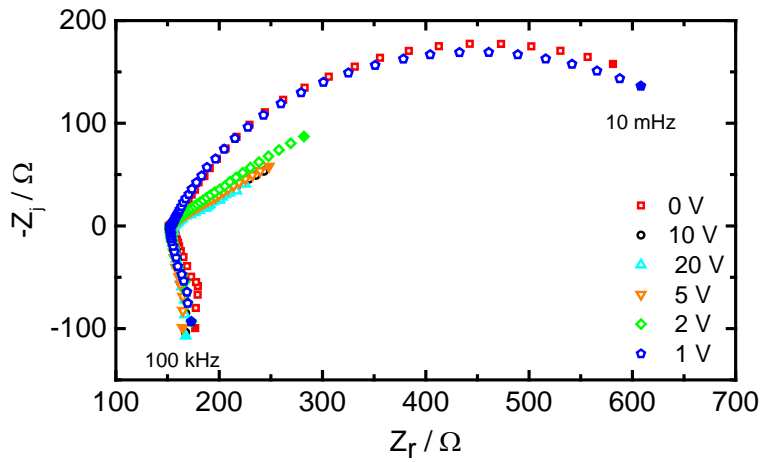
Figure 7. Four-point experimental impedance during the application of a constant potential difference between the steel and a surface electrode located at the center of the specimen.
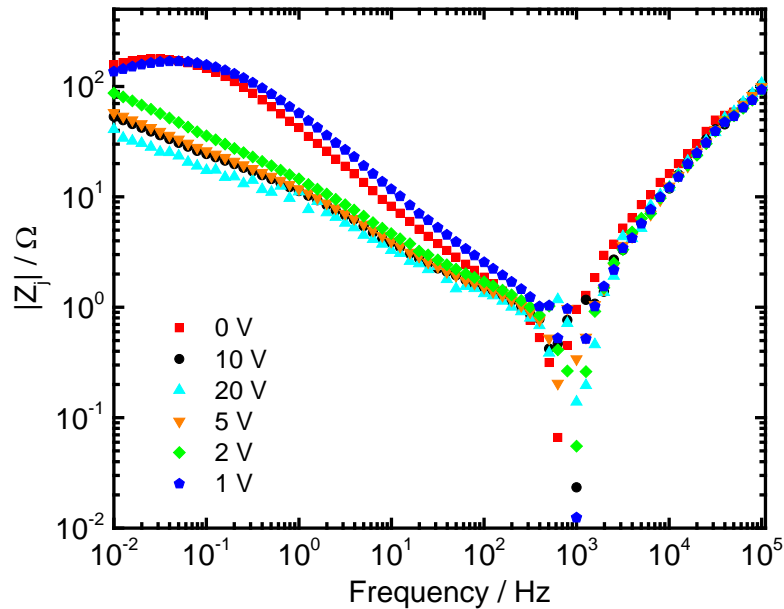
Figure 8. Four-point experimental imaginary impedance as a function of frequency during the application of a constant potential difference between the steel and a surface electrode located at the center of the specimen.

2.2. Finite-Element Model

Extraction of the steel impedance from the indirect impedance measurement requires knowledge of the resistivity of the grout, how it contributes to the overall impedance, the amount of steel surface area that is sensed, how the electrode kinetics affects the impedance, and how the location of the reference electrodes affects the measurement. Finite-element models were used to simulate the indirect impedance and develop interpretation techniques which address these issues. The simulated impedance was calculated from the oscillating potential distribution response and the applied current at the working electrode. The boundary conditions explained in the mathematical development were applied to a 2D square as a proof of concept and then to a 3D cylindrical specimen to represent a section of a tendon.

9

2.2.1. Mathematical Development

The indirect impedance technique requires a 4-electrode array consisting of a working and counter electrode (outer two electrodes of the array) and two reference electrodes (inner two electrodes of the array). An ac perturbation is applied between working and counter and the reference electrodes measure the potential response. The current follows an ac regime flowing back and forth between the working and counter electrode, taking the path of least resistance. Depending on the geometry of the specimen and the frequency of the perturbation, a certain fraction of the current will go solely through the grout while the rest will enter the steel. Therefore the steel is indirectly polarized due to the ac perturbation at the surface.

To aid in the interpretation of the experimental results, a finite-element model was developed to simulate the indirect impedance. Huang et al.[14] explains the use of linear kinetics as the boundary condition on a disk electrode based on the derivations of Newman[15] and Nisancioglu.[16,17] The normal current density at the surface of the electrode can be expressed in terms of a faradaic reaction and a charging current as

$$i = C\frac{\partial(V - \Phi)}{\partial t} + \frac{(\alpha_a + \alpha_c)i_0 F}{RT}(V - \Phi) = -\kappa\frac{\partial\Phi}{\partial y} \tag{2}$$

The oscillating current density may be expressed in the frequency domain as

$$\tilde{i} = j\omega C(\tilde{V} - \tilde{\Phi}) + \frac{(\alpha_a + \alpha_c)i_0 F}{RT}(\tilde{V} - \tilde{\Phi}) \tag{3}$$

with the use of the relationship

$$i = \bar{i} + \text{Re}\left\{\tilde{i}\, e^{jwt}\right\} \tag{4}$$

where the current is expressed as the addition of a steady-state and an oscillating term. In equation 3, $\tilde{V}$ is the potential perturbation, and $\tilde{\Phi}$ is the complex oscillating potential within the electrolyte. For the indirect impedance simulation both the working and counter electrode boundary conditions were set as oscillating currents with a positive potential perturbation applied to the working electrode and a negative one applied to the counter electrode. A similar boundary condition was set at the steel but with the potential set to zero so that all other potentials would be in reference to this. The steel was modeled for an active corrosion case and a passive blocking electrode case. The active case, equation 5, is expressed as the addition of the charging and faradaic current.

$$\tilde{i} = j\omega C(-\tilde{\Phi}) + \frac{(\alpha_a + \alpha_c)i_0 F}{RT}(-\tilde{\Phi}) \tag{5}$$

The passive case is modeled using a Constant-Phase-Element (CPE) with an impedance given by

$$Z_{CPE} = \frac{1}{(j\omega)^\alpha Q} \tag{6}$$

10

where the phase angle is independent of frequency. When $\alpha = 1$, Q has units of capacitance. When α does not equal 1, the system has a distribution of time constants or surface heterogeneity either normal or parallel to the surface.[18] The expression used to represent blocking behavior at the steel for the normal current density of a CPE is

$$\tilde{i} = -\tilde{\phi}\omega^{\alpha}Q\left[\cos\left(\alpha\frac{\pi}{2}\right) + j\sin\left(\alpha\frac{\pi}{2}\right)\right] \tag{7}$$

The oscillating potential solution was found by solving Laplace's equation with the given frequency-dependent boundary conditions. With the use of potential probes, the impedance is simulated as the quotient of the potential difference between two reference probes and the current perturbation applied between the current-injecting electrodes, expressed as

$$Z = \Delta V / \Delta I \tag{8}$$

The charge-transfer resistance for linear kinetics can be expressed in terms of the exchange current density as

$$R_t = \frac{RT}{i_0\left(\alpha_a + \alpha_c\right)} \tag{9}$$

which is the same expression used to estimate the polarization resistance of the steel in the corroding case. The 3D potential distribution was determined assuming a uniform conductivity electrolyte, and the indirect impedance was simulated.

2.2.2. Justification of Boundary Conditions

A 2D square of uniform conductivity, Figure 9, was modeled to confirm the oscillating current boundary conditions. The vertical sides of the square acted as the current-injecting electrodes. The potential distribution is shown by the color gradient in Figure 9 and the current path is shown by the horizontal red lines. The 2-pt impedance was simulated by dividing the potential difference between the electrodes by the total current crossing one of the electrode boundaries. At all frequencies, the real impedance, Figure 10, is the resistivity of the electrolyte multiplied by the distance between the electrodes and divided by the cross-sectional area. The imaginary impedance is zero since the grout is modeled as a homogenous material with a constant resistance without any dielectric properties.
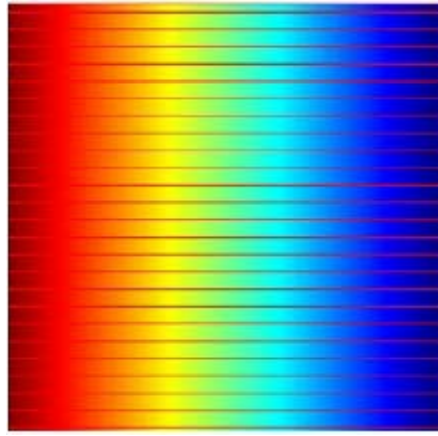
Figure 9. Current and potential distribution of a 1-cm-square, 10-Ohm-m resistivity grout model with current injecting electrodes placed on the vertical sides.
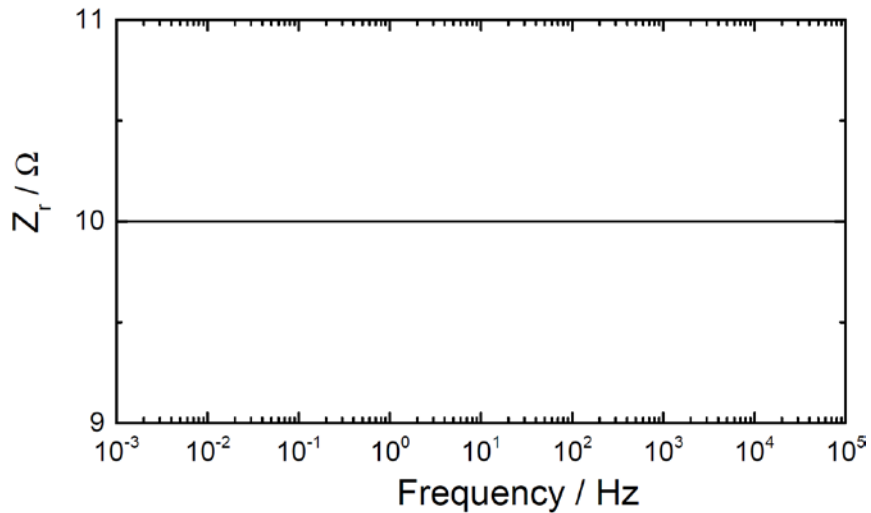
Figure 10. Simulated real impedance of as a function of frequency of a 1-cm-square grout model with current injecting electrodes placed on the vertical sides. The imaginary part of the impedance is equal to zero and the real part of the impedance is equal to 10 Ohms.

An actively corroding steel circular element was inserted into the grout model with the boundary condition described by Equation 5. At low frequencies, Figure 11a, the steel behaves as an open circuit due to the dominance of the charge-transfer resistance and repels the current. At high frequencies, Figure 11b, it behaves as a closed-circuit and the current enters it normal to the surface. These results are consistent with those of Keddam et al.[13] The Nyquist plot of the simulated impedance, Figure 12, is a capacitive semi-circle representative of a resistor and a capacitor in parallel. This is a simple model that shows the concept of indirect impedance, and confirms the use of the oscillating boundary conditions.
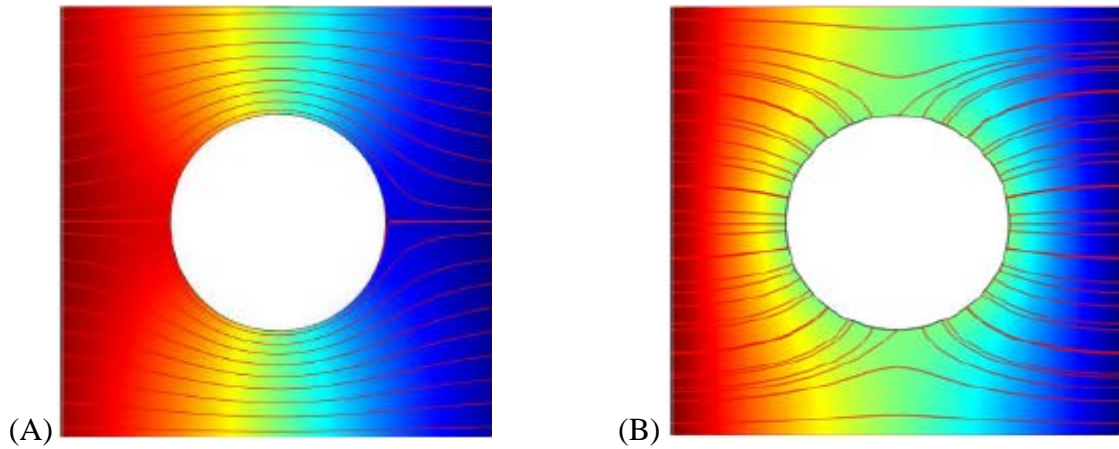
Figure 11. Current and potential distribution of a 1-cm-square grout model with a 0.25-cm radius steel placed in the center and current injecting electrodes placed on the vertical sides at the (A) low-frequency and (B) high-frequency limits.
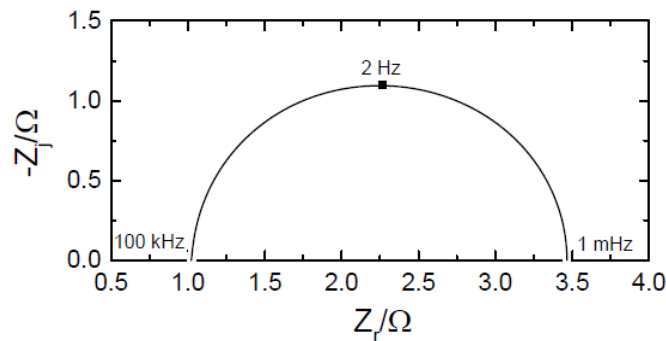
Figure 12. Simulated impedance of a 1-cm-square grout model with a 0.25-cm radius steel circle placed in the center and current injecting electrodes placed on the vertical sides.

A three-dimensional, 60cm long cylindrical section of a tendon was modeled, to simulate the impedance of a post-tensioned tendon. The steel strand is 0.625 cm in radius and is located along the longitudinal axis of the cylinder. All dimensions of the model were made to match the fabricated tendons. The mesh of the model, Figure 13, is composed of free tetrahedral elements which decrease in size at the electrode boundaries. Boundary layer elements were added to the steel and electrode boundaries. Reference probes were placed along the surface to analyze the potential distribution.
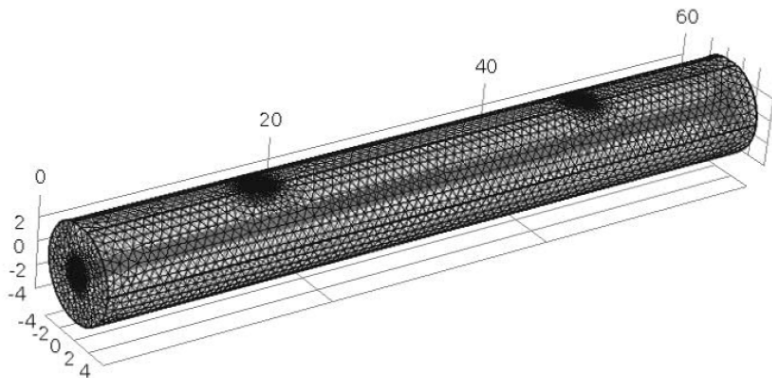
Figure 13. Mesh of the 3D tendon model.

13

2.2.3. Experimental Data Fitting

The passive case simulation was used to fit the experimental impedance by first estimating the resistivity of the grout as 125 Ohm-m and iterating the CPE parameters at the steel. The CPE parameter associated with the double layer Q was found to be 0.9 Ss^{α} and α was 0.9. The simulated impedance is shown to fit the experimental data of two electrode configurations at low frequencies, provided in Figures 14 and 15. The high-frequency time constant is not fully understood at this time. Nevertheless, the fitting of the low-frequency behavior is a validation of our finite element model in its ability to replicate experimental measurements and, therefore, may be used to establish an interpretation procedure.
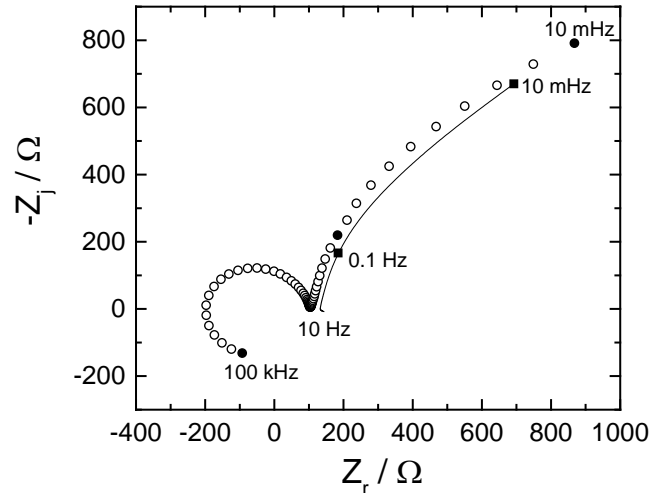
Figure 14. Simulated impedance results compared to the experimental results with an electrode configuration of 2356.

Figure 15. Simulated impedance results compared to the experimental results with an electrode configuration of 1357.

2.2.4. Determination of Steel Sensing Area

The area of steel that is sensed for each electrode arrangement is required for the interpretation. The indirect impedance was simulated for 3 different cases: a fully passive steel strand, a uniformly corroding steel strand, and a passive strand with a localized area of corrosion at the center indicated by the red section in Figure 16. Twenty-five electr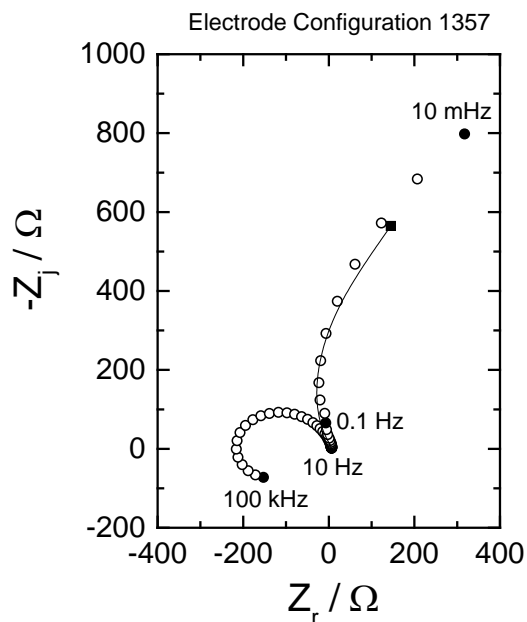ode points were placed along the surface such that multiple electrode configurations could be simulated at once. The steel boundary was broken into 60, 1-cm increments so that the current and potential at the steel could be determined along its length. The current entering or leaving the steel was taken to be the normal current at each point along the steel surface, i.e., the radial component of the current. The current distribution along the steel for each frequency allows for the estimation of the polarized steel area.

In one set of simulations the electrodes were placed with the centerline of the array directly over the active site. The distance between the two reference electrodes was varied from 32 cm to 4 cm to determine if there is a maximum distance in which the corrosion could not be detected. When the electrodes were spaced far apart, the difference between the passive case and the locally corroding case was extremely small. As the electrodes were moved closer together the difference increased but even when the reference electrodes were placed just above the active location, Figure 17, the impedance of the locally corroding case alone did not indicate the presence of corrosion. However, the presence of a small difference even when the reference electrode distance is 32 cm indicates that the polarized steel area extends far out from the electrode points, but the location of steel most sensed is not at the centerline of the electrode array.
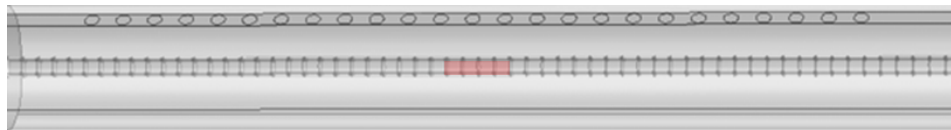
Figure 16. Tendon model with locally corroding section in the center of the steel.

(A)

(B)

Figure 17. Simulated indirect impedance of a 2-ft model tendon containing one steel strand for a passive case, a locally corroding case of 4 cm at the midpoint of the steel strand, and a uniformly corroding steel: (A) impedance results; and (B) schematic representation of the system geometry for a reference electrode spacing of 4 cm.

15

In the next set of simulations, the electrodes were equally spaced at 4 cm and were moved along the tendon to mimic a likely procedure for a field application. In this case, when the midpoint of the electrode array was 18 cm left of the active location, the impedance of the passively and actively corroding cases showed only small differences at lower frequencies. When the electrodes were located 10 cm from the corroding section, the difference became more apparent. However, when one of the reference electrodes was directly over the site of corrosion, the difference diminished. The most prominent difference occurred when the current-injection electrode was directly over the site of corrosion, as is shown in Figure 18.

This behavior can be explained by assessing the current distribution along the steel. Figure 19a shows the current distribution at 100 Hz, and Figure 19b is the current distribution at 10 mHz. At 100 Hz, the current entering the steel is confined to two distinct locations directly underneath the working and counter electrodes, the maximum current being on the order of 10^{-4} A. At 10 mHz, the current is spread out over the whole length of the steel, entering in one half of the steel and exiting at the other half. With the total sensing area of the steel increasing as the frequency decreases, the total steel impedance would decrease as the frequency increases.
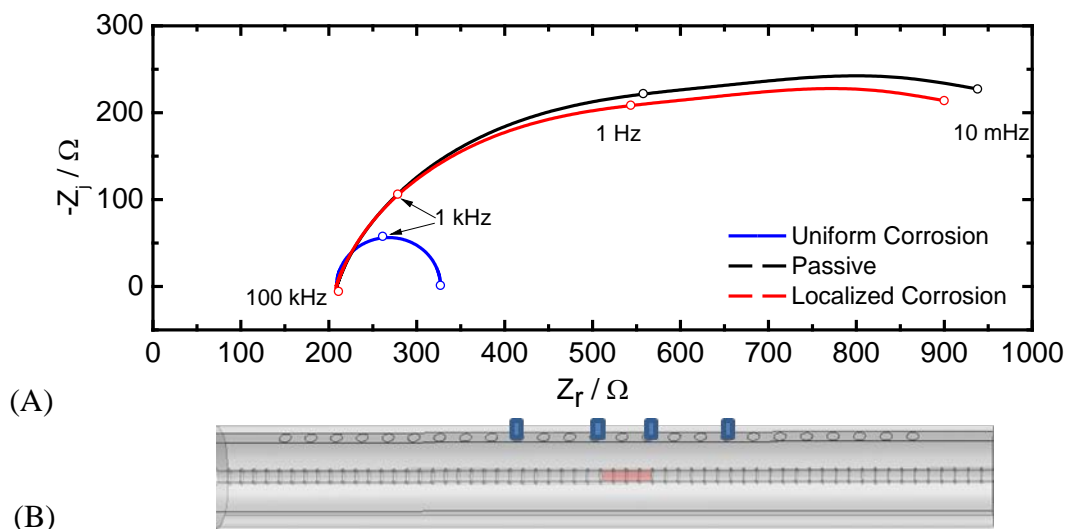

a)

b)
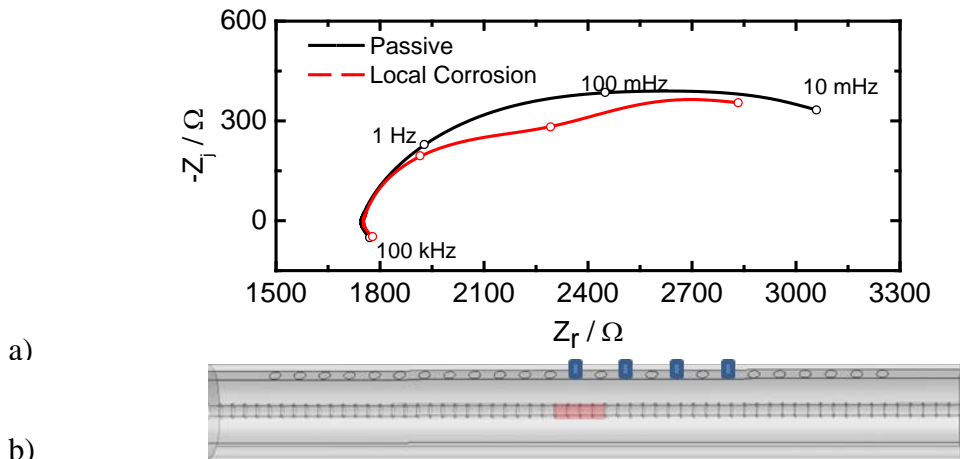
Figure 18. Simulated indirect impedance of a 2-ft model tendon containing one steel strand for a passive case and a locally corroding case of 4 cm at the midpoint of the steel strand. The centerline of the electrode array is 6 cm right of the centerline of the 2-ft tendon, and the working electrode is directly over the corroding area: a) impedance results; and b) schematic representation of the system geometry for a reference electrode spacing of 4 cm.

a)

b)
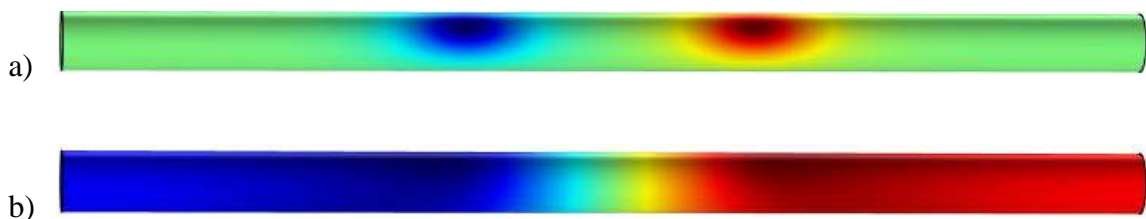
Figure 19. Current distribution on the steel surface for the passive case at (a) 100 Hz and (b) 10 mHz.

The polarized area of steel is also dependent on the impedance of the steel. Figures 20a and b show the current distribution on the steel for 100 Hz and 10 mHz for a uniformly corroding steel and in this case at low frequency the sensing area increases some but does not extend to the entire length of steel. This phenomenon is also illustrated in Figure 21 where the current at the steel is plotted as a function of axial position for the active and passive case. Again, in the passive case the current extends to both ends of the steel strand, but in the active case, the current is still confined to the two locations directly beneath the current electrodes.

a)

b)

Figure 20. Current distribution on the steel surface at (a) 100 Hz and (b) 10 mHz for the active case.

Figure 21. Current distribution on the steel surface at as a function of steel position at 10 mHz.
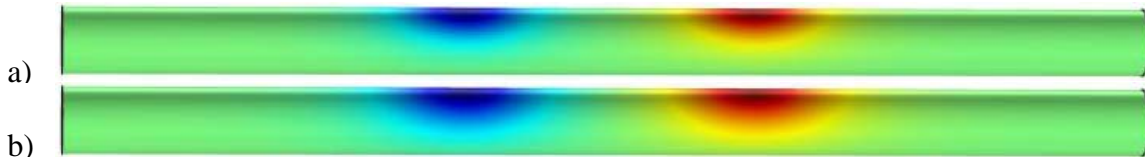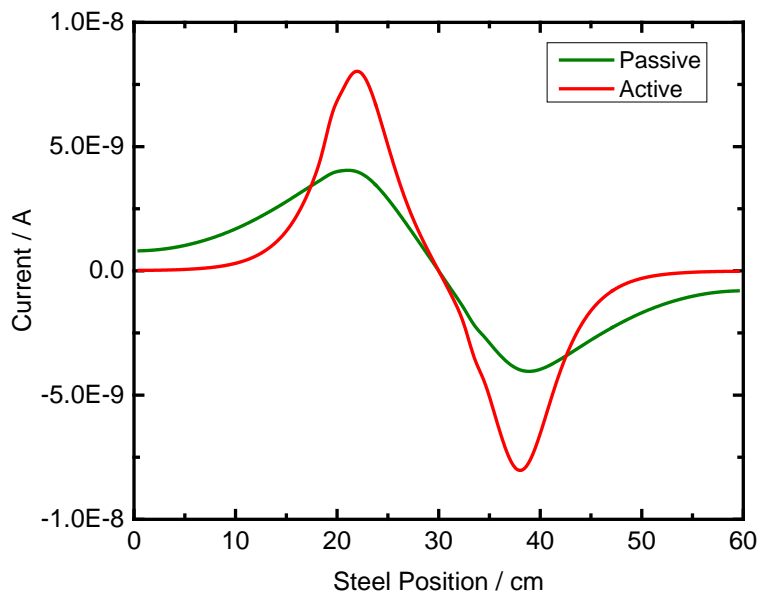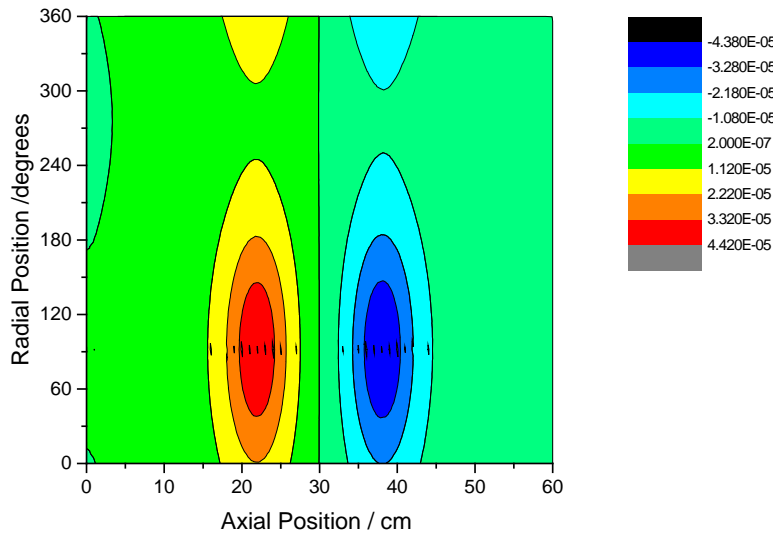
Figure 22. Current on the steel surface at 100 Hz.

The current at the surface of the steel is plotted in 2D in Figure 22. From this diagram the polarized area of steel can be estimated as the total area of all colors excluding the color green. At this frequency, that area is approximately 157 cm^2. Notice that the polarized area is confined to the top portion of the steel and does not reach the bottom of the steel indicated by the current at $\theta = 270$ degrees. This shows that if there is corrosion present on the underside of the steel, it may go undetected.

Also, while this may represent the total polarized surface area of steel, the actual sensing area may be influenced by the location of the reference electrodes. One hypothesis of how the potential probe location affects the sensing area is that the potential at the location of the reference electrodes is a fraction of the total potential difference that would be measured between the current-injecting electrodes, and, therefore, the sensing area is the total polarized area scaled by this percentage and the magnitude of the impedance is also scaled by this percentage. To test this, the potential percentage was determined for two different reference electrode distances as a function of frequency, presented in Figure 23. This percentage was used to scale the magnitude of one of the impedance simulations to determine if it matched the magnitude of the other. The results are presented in Figure 24 in which the scaled magnitude of the impedance is plotted as a function of frequency and is compared to the second impedance for both the passive and active cases. At high frequencies the scaled impedance matches the magnitude of the impedance of the other simulated impedance but there is deviation at lower frequencies. If the difference is taken between the two and plotted with the imaginary impedance of one of the simulations it can be seen that the time constant associated with both is the same as displayed in Figure 25. This indicates that the location of the reference electrodes affects the total area of steel sensed. If this was not the case, the scaled impedance would match the impedance of the second reference electrode spacing. How the location of the reference electrodes affects this area will be the topic of future research. This parameter will be important in the extraction of the steel impedance from the indirect impedance measurement.
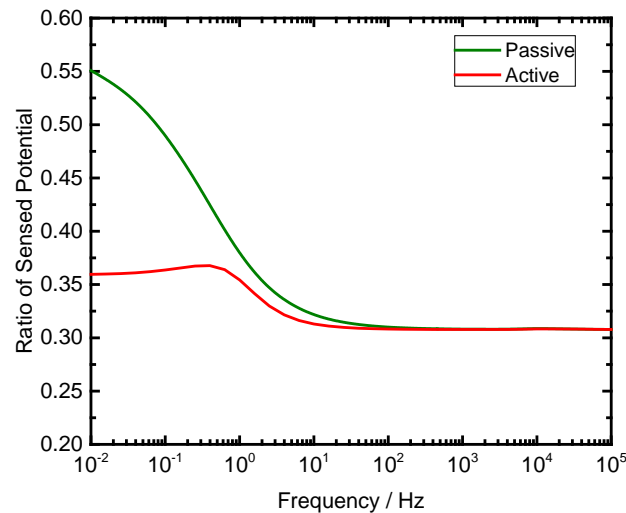
Figure 23. The ratio of the potential sensed between two impedance measurements where only the distance between reference electrodes is changed for the active and passive case.

18
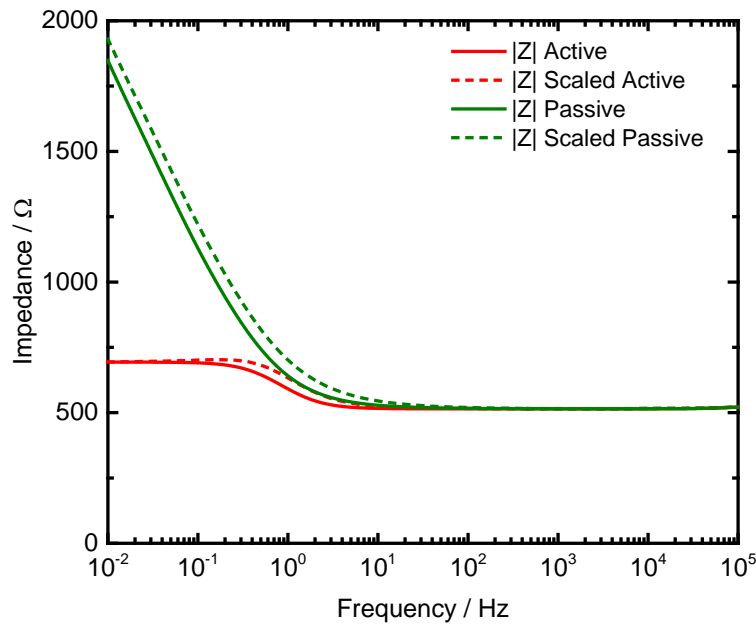
Figure 24. Magnitude of the impedance scaled by the potential ratio of two different reference points compared to the magnitude of the impedance measured with the second reference point as a function of frequency for the passive and active cases.
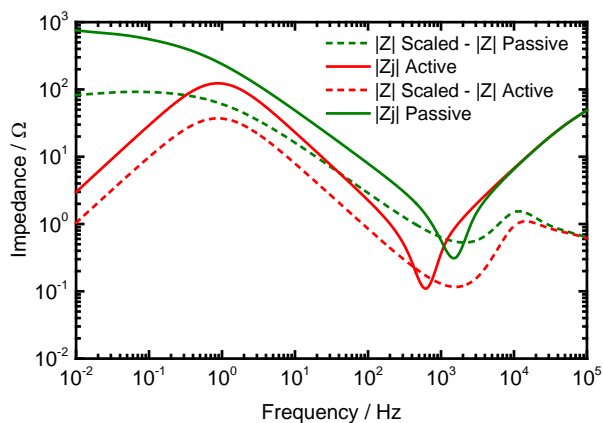
Figure 25. Difference in the magnitude of the potential scaled impedance and the magnitude of the impedance taken with the second reference point compared to the absolute value of the imaginary impedance taken with the second reference point as a function of frequency for the active and passive cases.

2.2.5. Circuit Analysis

During the indirect impedance measurement, current flows through the grout as well as through the steel. If the contribution of the grout resistivity to the indirect impedance can be determined then the total steel impedance may be extracted. Andrade et al.[10] proposed the use of an analogue circuit to describe the indirect impedance measurement of reinforced concrete. They determined that a suitable circuit must contain a parallel as well as a series resistance term associated with the resistivity of the concrete in relation to the impedance of the steel.

The impedance response of the circuit shown in Figure 26 was compared to the impedance obtained by numerical finite-element simulations. The current distribution results provided by our

19
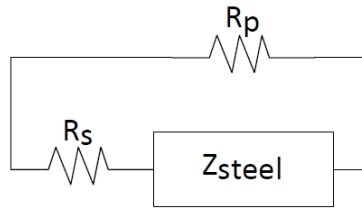
Figure 26. Circuit representation of indirect impedance.

finite-element simulations show that there are two possible paths the current can take. It can go solely through the grout or it can go through the grout and then through the steel. Since some of the current can take one path while the rest takes the other, these two cases must be in parallel.

From this circuit analysis, it was determined that the series resistance is a function of the depth to the steel. In all electrode configurations tested, the parallel resistance was much greater than the series resistance, showing the likelihood of the current to go through the steel. The parallel resistance was determined to be reliant on the distance between the working and counter electrodes. It was not found to be a direct function of the steel cross-sectional area because most of the current that goes through the grout is located close to the top surface of the grout. Since the series resistance cannot be controlled by the electrode spacing, an appropriate electrode configuration has a large working and counter electrode spacing, and a large enough spacing between the reference electrodes to eliminate distortions due to potential distributions.

2.3. Convectional Bench-top Impedance Measurement

Conventional bench-top experiments are aimed to understand the corrosion behavior and electrochemistry of ASTM A416 within the tendon. All experiments were conducted with a three electrode setup. The electrochemical behavior of ASTM A416 steel was studied by electrochemical impedance spectroscopy. Simulated pore solutions, based on the recipe presented by Li and Sagues,[19] were used as the electrolyte for all experiments. Its composition is presented in Table 1. The summaries of the convectional bench-top impedance measurements are list below:

1. Dissolved oxygen has more influence on corrosion rate than chloride ions.
2. Increased temperatures caused increases in the corrosion rate.
3. The corrosion reaction of steel is very sensitive to the oxygen content. Experiments exposed to air by an open surface eventually became depleted of oxygen, changing the corrosion potential and the impedance response. New experiments require active aeration to replace depleted oxygen and active de-aeration to avoid air ingress.

Table 1. Chemical composition and pH value of test solution (g/L)

SPS	$Ca(OH)_2$	NaOH	KOH	pH	NaCl	Deaerated
A	2	8.33	23.3	13.6	0	no
B	2	8.33	23.3	13.6	40	no
C	2	8.33	23.3	13.6	0	yes
D	2	8.33	23.3	13.6	40	yes

2.3.1. Corrosion Study from Impedance Measurement

All electrochemical impedance diagrams were recorded at the corrosion potential, E_{corr}, after the electrode was conditioned for one hour at -1 V and then held at the open circuit condition for one

hour. The impedance scans can be represented by two capacitive loops, a high-frequency (HF) loop with low capacitance, and a low-frequency (LF) loop which may include the diffusion impedance. The impedance response of steel in chloride-free aerated electrolytes (SPS-A) is presented in Figure 33 with elapsed time as a parameter. After an immersion time of one hour, the low-frequency feature was a straight line with an angle of approximately 22.5 degrees with respect to the real axis. After an elapsed time of 18 hours, the size of the high-frequency capacitive loop increased, and the angle of the low-frequency line approached 45 degrees. After 36 hours, the size of the high-frequency capacitive loop decreased, and the angle of the low-frequency line was 43 degrees. The impedance response of steel in aerated electrolytes with 40 g/L (0.68 M) NaCl (SPS-B) is presented in Figure 34 with elapsed time as a parameter. After an immersion time of one hour, the low-frequency feature was a straight line with an angle of 25 degrees with respect to the real axis. After an elapsed time of 18 hours, the size of the high-frequency capacitive loop increased, and the angle of the low-frequency line approached 45 degrees. After 36 hours, the size of the high-frequency capacitive loop increased, and the angle of the low-frequency line was 40 degrees. The impedance data showed similar behavior as compared to that seen in chloride-free electrolytes (Figure 33). This result suggests that, even when the chloride concentration is higher than the chloride threshold level, no corrosion damage can occur if the surface potential remains lower than the pitting potential.

The impedance response of steel in chloride-free de-aerated electrolytes (SPS-C) is presented in Figure 35 with elapsed time as a parameter. After one hour, the low-frequency feature was a straight line with an angle of 26 degrees with respect to the real axis. In contrast to the results obtained in aerated electrolytes (Figures 33 and 34), the low-frequency line remained at 26 or 27 degrees, even after 36 hours. The high-frequency capacitive loop increased for scans from 1 to 16.5 hours elapsed time, but did not change between 16.5 and 36 hours elapsed time.

The impedance response of steel in de-aerated electrolytes with 40 g/L NaCl(SPS-D) is presented in Figure 36 with elapsed time as a parameter. After one hour, the low-frequency feature was a straight line with an angle of 22.5 degrees with respect to the real axis. After 18 hours, the low-frequency feature had a slight curvature. The curvature of the low-frequency feature was more pronounced at 36 hours, and its high-frequency slope with respect to the real axis was 37 degrees. In spite of the curvature of the low-frequency loop, steel immersed in this electrolyte showed no visible corrosion. This result is in agreement with observations in other aerated and de-aerated electrolytes. These results suggest that dissolved oxygen content did affect the corrosion behavior of ASTM A416 steel. Steel immersed in aerated electrolyte can form a well-protective oxide film, while in de-aerated electrolytes the oxide film still shows porous electrode behavior. Temperature effect has also been studied by electrochemical impedance spectroscopy. Figure 37 shows the impedance response for steel immersed in aerated chloride-free electrolyte with temperature as parameters. Impedance results suggest that porous electrode behavior was visible for temperatures 10° C and 25° C. However, at 40° C, porous electrode behavior was not visible. The details of the porous electrode model will be discussed in following section.

Figure 27. Impedance response of the ASTM A416 steel at the open-circuit potential immersed in chloride-free aerated solution (SPS-A) with elapsed time as a parameter.

Figure 28. Impedance response of the ASTM A416 steel at the open-circuit potential steel immersed in 40 g/L chloride aerated solution (SPS-B) with elapsed time as a parameter.
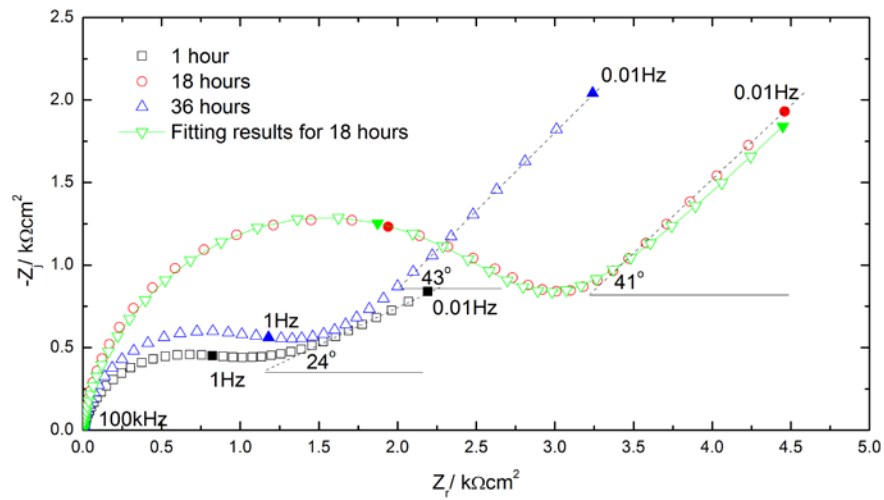
22
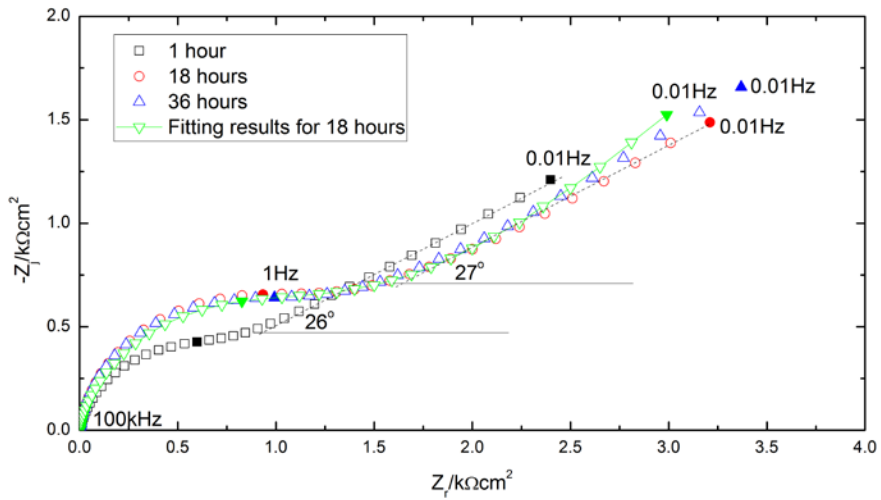
Figure 29. Impedance response of the ASTM A416 steel at the open-circuit potential immersed in chloride-free deaerated solution (SPS-C) with elapsed time as a parameter.
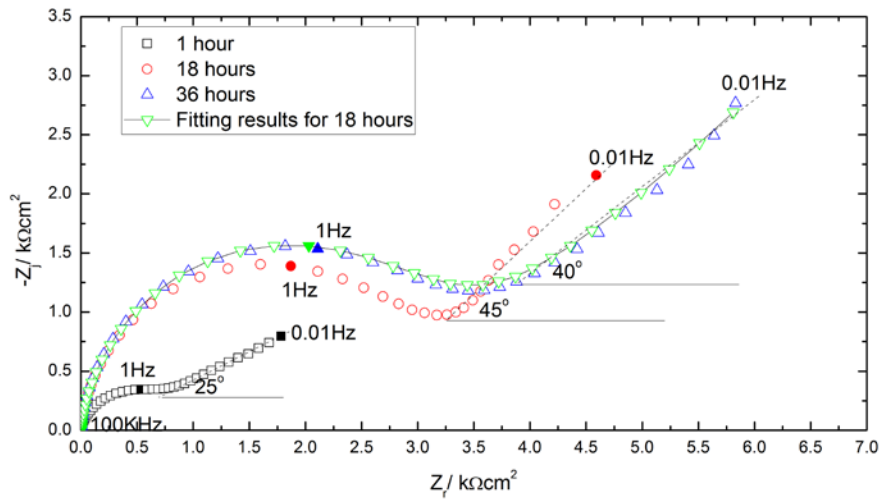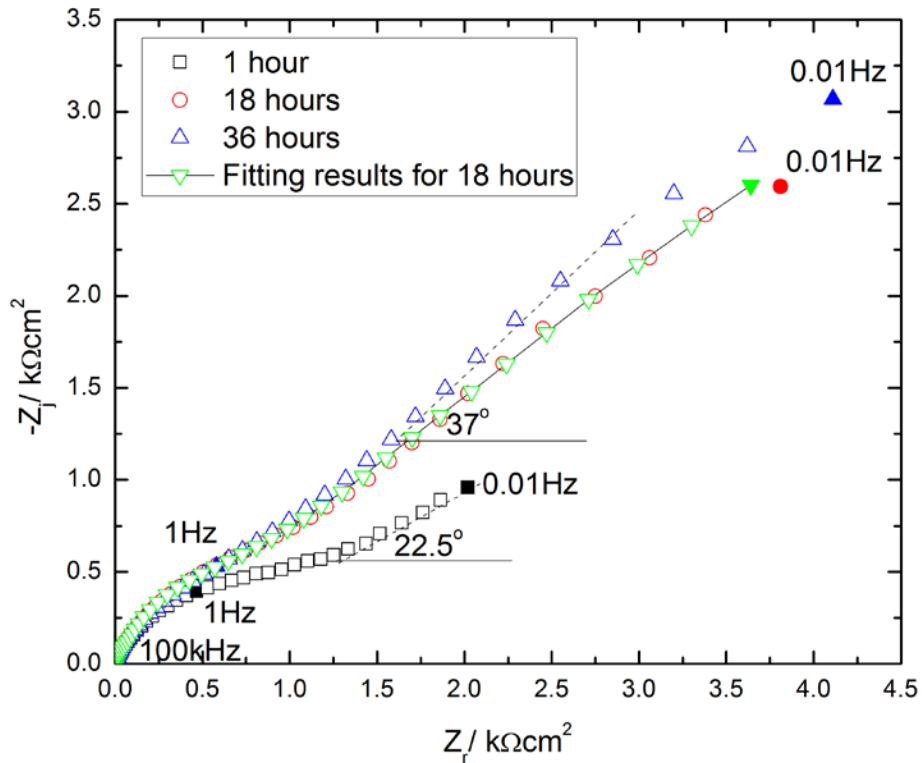

Figure 30. Impedance response of the ASTM A416 steel at the open-circuit potential steel immersed in 40 g/L chloride deaerated solution (SPS-D) with elapsed time as a parameter.

23
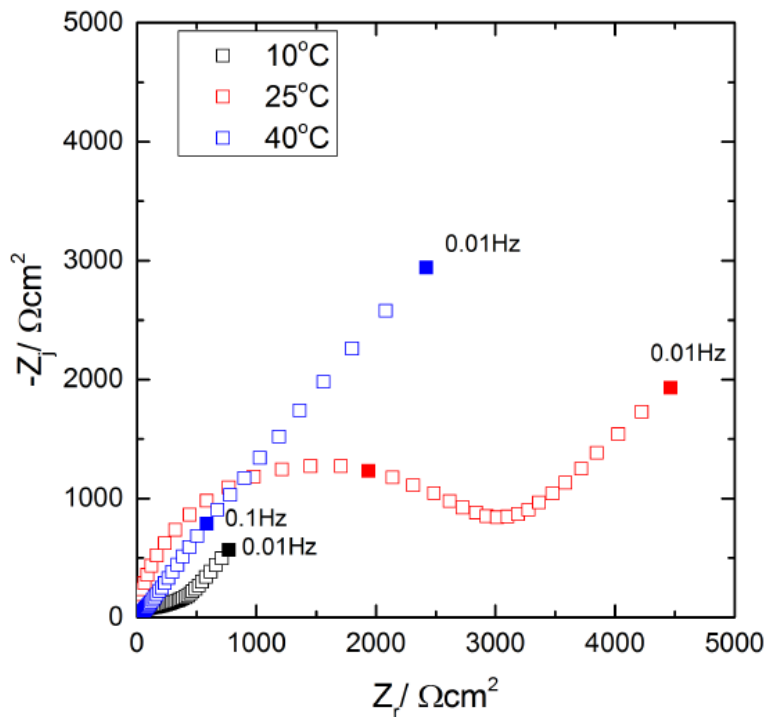
Figure 31. Impedance response of the ASTM A416 steel at the open-circuit potential steel immersed in aerated solution with temperature as a parameter.

2.3.2. Open-Circuit Potential Study

The long term corrosion behavior was studied by open-circuit potential. From Figure 38, open-circuit potential for SPS-A exposed to air by an open surface eventually became depleted of oxygen after around 10,000 seconds, changing the corrosion potential and the impedance response. New experiments require active aeration to replace depleted oxygen and active de-aeration to avoid air ingress.
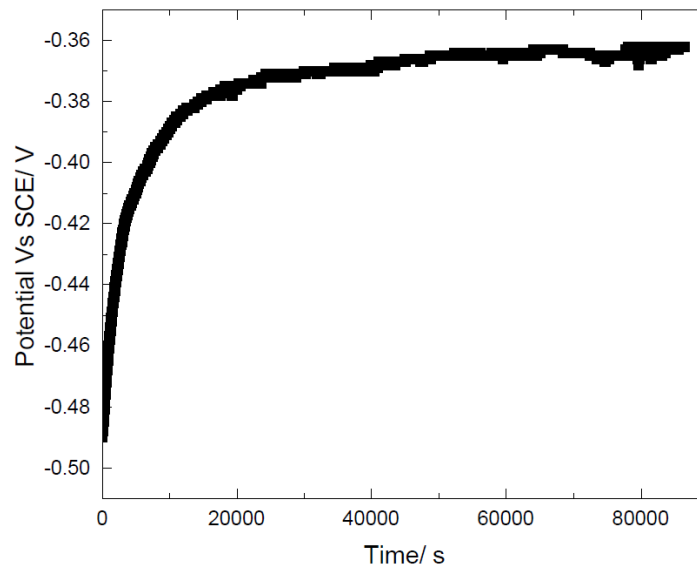
Figure 32. Open-circuit potential of the ASTM A416 steel in SPS-A as function of time.

24

2.4. Mathematical Models

Under the assumption that the anodic reaction follows Tafel kinetics, the anodic impedance, Z_a, can be regarded to be a double layer capacitance, $C_{a,dl}$ in parallel with a charge-transfer resistance, $R_{a,t}$, as shown in Figure 39b. The cathodic branch is based on a porous electrode model, which has an impedance distributed in space as a transmission line in the conducting macro-pore (Figure 40). This transmission line is composed of the elementary elements $R_0\Delta x$ and $Z_0/\Delta x$, where R_0 is the ohmic drop resistance for a unit length macro-pore (in Ω cm^{-1}), Δx is the thickness of an infinitesimal slice of the macro-pore and Z_0 is the interfacial impedance for a unit length macro-pore (in Ω cm).

As shown in Figure 39c, the interfacial impedance Z_0 is composed of a parallel arrangement of the cathodic double layer capacitance, $C_{c,dl}$ and the faradaic branch consisting of a cathodic charge transfer resistance, $R_{c,t}$ in series with a diffusion impedance Z_D. The term, Z_D, which describes the radial diffusion in the macro-pores, is given by Drossbach and Schulz[20] to be

$$Z_D = R_D \frac{\tanh\left(\sqrt{j\omega \frac{\delta_r^2}{D_r}}\right)}{\sqrt{j\omega \frac{\delta_r^2}{D_r}}} \tag{10}$$

where R_D is the diffusion resistance (Ω), δ_r the thickness of the diffusion layer (cm) and D_r the diffusivity of dissolved oxygen in pore (cm^2 s^{-1}).

The cathodic impedance has the general form

$$Z_C = \sqrt{R_0 Z_0} \coth\left(\frac{L}{\lambda}\right) \tag{11}$$

where

$$\lambda = \sqrt{\frac{Z_0}{R_0}} \tag{12}$$

The specific impedances R_0 and Z_0 can be expressed in function of the pore radius as

$$R_0 = \frac{\rho}{\pi r^2} \tag{13}$$

and

$$Z_0 = \frac{Z_{eq}}{2\pi r} \tag{14}$$

where Z_{eq} is the interfacial impedance per surface unit, with units Ωcm^2, ρ is the electrolyte resistance, with units Ωcm, and r is the pore radius in cm. The mean length of the macro-pores is

25

L and the penetration depth of the electrical signal is λ. When L is small with respect to λ, the macro-pores respond like a flat electrode and the cathodic impedance tends to Z_0/L. In this case, the angle made by the diffusion impedance is equal to $45°$. When L/λ becomes large, the macro-pores behave as though they were semi-infinitely deep. Thus, for large L/λ, $\coth(L/\lambda)$ tends to unity, and Z_C equals $(R_0 Z_0)^{1/2}$, which gives an angle of about $22.5°\,C$ in the so-called Warburg domain.

The impedance data fitted by the porous electrode model was shown in Figures 33-36. The fitting results suggest that this model works well for all the cases. For results at $10°\,C$, the anodic reaction impedance cannot be seen; whereas, at $40°\,C$ the cathodic reaction impedance cannot be seen. For both cases, an outer film impedance response was observed. From the results, the corrosion rate of steel immersed in de-aerated simulated pore solution with 40 g/L NaCl at $25°\,C$, is about 7 µm/year. For other cases in room temperature, corrosion rates are too small to be measured. However, when the steel immersed in aerated simulated pore solution with 40 g/L NaCl at $40°\,C$, the corrosion rate can reach about 30 µm/year. This behavior suggests that temperature has more influence on corrosion rate than added chloride ions.
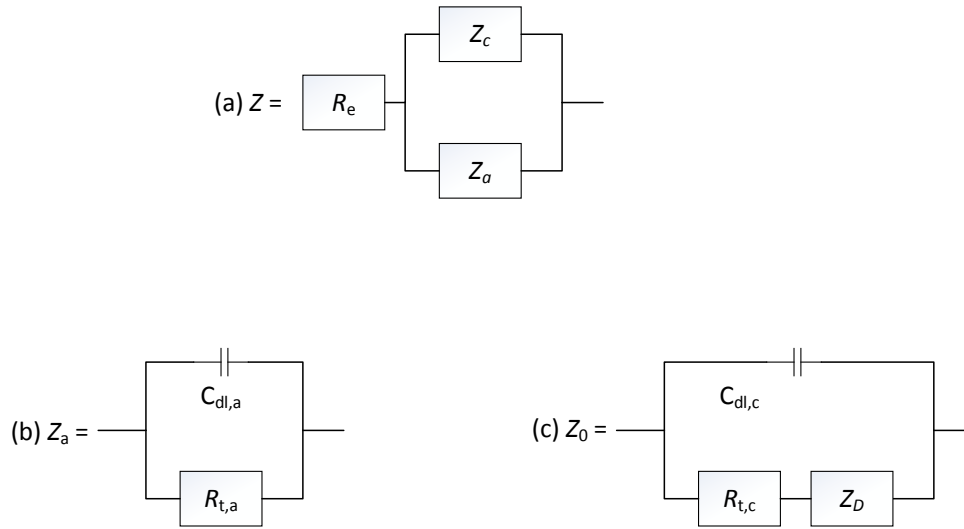

Figure 33. Equivalent circuit for (a) total impedance of the steel/simulated pore solution interface, (b) anodic impedance, (c) interfacial impedance of the micro-porous layer.
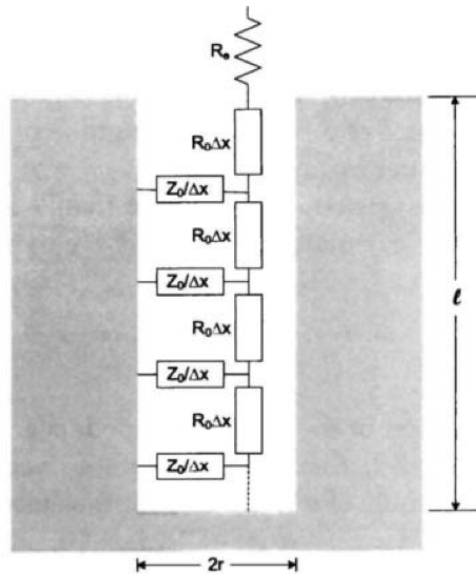
Figure 34. Schematic representations of a porous electrode: transmission line inside a cylindrical pore. Taken from Orazem and Tribollet.[18]

3. Breakdown of Effort Allocated to Work

An estimate of the effort breakdown is presented in Table 2.

Table 2. Breakdown of experiments and hours spent on each task

Simulated pore solution experiments	# of disk electrodes fabricated	8
	# of electrolyte solutions tested	7
	# of temperatures	3
	# of rotation speeds	4
	# of EIS measurement	~900
	Model development time	~120 h
	Regression analysis time	~200 h
Synthetic tendon experiments	# of Synthetic tendons made	23
	# of EIS measurements - 6 electrode configurations - 5 environments	~850
	# of COMSOL Simulations	~750
	Simulation computation time	~8500 h
	Model development time	~450 h
	Regression and simulation analysis time	~650 h
Literature review	Literature review time	~600 h
	Papers read	~450
	Papers directly applicable to project	~60

4. Project Schedule

Table 3. Project Schedule

FLORIDA DEPARTMENT OF TRANSPORTATION

RESEARCH CENTER

PROJECT SCHEDULE

Project Title	Impedance-Based Detection of Corrosion in Post-Tensioned Cables: Phase 1 Extension. Sensor Development									
FDOT Project No.	TBD								FY	2014	Month	September
Research Agency	University of Florida											
Principal Investigator	Mark E. Orazem and David Bloomquist, P.E.											

RESEARCH	March	April	May	June	July	August	September	October			ESTIMATED %
TASK	2014	2014	2014	2014	2014	2014	2014	2014			COMPLETION
Interim Task: The validity of the impedance-based sensor for detecting corrosion in tendons is based on a series of laboratory and computational studies. An interim report will provide a summary of the results of these studies, including mathematical models to interpret the impedance of corroding strands, bench-top contact-less impedance experiments on simulated strands, and bench-top experiments conducted in simulated pore solutions.	33 % complete	67% complete	100% complete								100%
Final Task: Ninety (90) days prior to the end date of the task work order, the university will submit a draft final report to sandra.bell@dot.state.fl.us. The draft final report will contain a description of the sensor design and the supporting research. The final report will cover and include the work from the previous phase as well as for the present project.			33 % complete	67% complete	100% complete						100%
Final Task Review and revision											
Overall % Complete Projected			50%		90%			100%			
Overall % Complete Actual			50%		90%			100%			

29

5. References

1. W. H. Hartt and S. Venugopalan, *Corrosion Evaluation Of Post-tensioned Tendons on the mid bay bridge in Destin, Florida*, (FDOT Research Project). Florida Atlantic University, Dania Beach, Florida, 2002

2. A. A. Sagues and S.C. Kranc, *Initial Development of Methods for Assessing Condition of Post-tensioned Tendons of Segmental Bridges*, (FDOT Research Project BC374). University of South Florida, Tampa, Florida, 2000

3. R. G. Powers, A. A. Sagues, Y. P. Virmani, *Corrosion of Post-tensioned Tendons in Florida Bridges*, (FDOT Research Report No. FL/DOT/SMO/04-475). Florida Department of Transportation, Gainesville, Florida, 1999

4. Corven, J., *Mid-Bay Bridge Post-Tensioning Evaluation*, (FDOT Final Report), Corven Engineering Incorporated, Tallahassee, October 2001.

5. A. A. Sagues, R. G. Powers, H. Wang, "Mechanism of corrosion of steel strands in post tensioned grouted assemblies," *Corrosion*, (2003).

6. A. Ghorbanpoor, "Magnetic-Based NDE of Pre-stressed and Post-Tensioned Concrete Members - The MFL System," *FHWA Technical Brief*, (2000).

7. P. Y. Virmani, "Literature Review of Chloride Threshold Values for Grouted Post-Tensioned Tendons," *FHWA Technical Brief*, (2012).

8. M. Stern and A. L Geary, "Electrochemical Polarization: I. A Theoretical Analysis of the Shape of Polarization Curves," *Journal of The Electrochemical Society,* **104** (1957), 56-63.

9. C. Andrade, I. Martinez, M. Castellote, "Feasibility of determining corrosion rates by means of stray current-induced polarisation," *Journal of Applied Electrochemistry*, **38** (2008) 1467-1476.

10. C. Andrade, J. Sanchez, I. Martinez, N. Rebolledo, "Analogue circuit of the inductive polarization resistance," *Electrochimica Acta*, **56** (2011), 1874-1880.

11. C. Andrade and I. Martinez, "Metal corrosion rate determination of different solutions and reinforced concrete specimens by means of a non-contacting corrosion method," *Corrosion*, **66** (2010) 05600-1 – 05600-10.

12. P. J. M. Monteiro and H. F. Morrison, "Nondestructive method of determining the position and condition of reinforcing steel in concrete," *US Patent*, **5855721 A** (1999).

13. M. Keddam, X. Nvoa, V. Vivier, "The concept of floating electrode for contact-less electrochemical measurements: Application to reinforcing steel-bar corrosion in concrete," *Corrosion Science*, **51** (2009), 1795-1801.

14. V. M. W. Huang, V. Vivier, M. E. Orazem, N. Pbre, B. Tribollet, "The apparent constant-phase-element behavior of a disk electrode with faradaic reactions a global and local impedance analysis," *Journal of the Electrochemical Society*, **154** (2007), C99-C107.

15. J. S. Newman, "Frequency dispersion in capacity measurements at a disk electrode," *Journal of the Electrochemical Society,* **117** (1970), 198-203.

16. K. Nisancioglu, "Theoretical problems related to ohmic resistance compensation," *The Measurement and Correction of Electrolyte Resistance in Electrochemical Tests,* ASTM STP 1056, L. L. Scribner, S. R. Taylor (Eds.), Philadelphia, PA, (1990), 61-77.

17. K. Nisancioglu, P. O. Gartland, T. Dahl, E. Sander, "Role of surface structure and low rate on the polarization of cathodically protected steel in seawater," *Corrosion,* **43** (1987), 710-718.

18. M. E. Orazem, B. Tribollet, *Electrochemical Impedance Spectroscopy,* John Wiley & Sons, Hoboken, NJ, 2008.

19. Lianfang Li, A.A. Sagüés, "Effect of Chloride Concentration on the Pitting and Repassivation Potentials of Reinforcing Steel in Alkaline Solutions," Paper 567, Proceedings of Corrosion/99, NACE International, Houston, Texas.

20. J. S. P. Drossbach, "Elektrochemische Untersuchungen an Kohleelektroden: 1. Die Überspannung des Wasserstoffs," *Electrochimica Acta*, **9** (1964), 1391-1404.